Available online at www.sciencedirect.com
SCIENCE DIRECT®
International Journal of Solids and Structures 43 (2006) 279–294
INTERNATIONAL JOURNAL OF SOLIDS and STRUCTURES
www.elsevier.com/locate/ijsolstr

Spectral element based model for wave propagation analysis in multi-wall carbon nanotubes

A. Chakraborty [a], M.S. Sivakumar [b], S. Gopalakrishnan [a,*]

[a] Department of Aerospace Engineering Indian Institute of Science, Bangalore 560 012, India
[b] Department of Applied Mechanics, Indian Institute of Technology, Chennai 600 036, India

Received 26 August 2004; received in revised form 14 March 2005
Available online 21 April 2005

Abstract

A spectrally formulated finite element is developed to study elastic waves in carbon nanotubes (CNT), where the frequency content of the exciting signal is at terahertz level. A multi-walled nanotube (MWNT) is modelled as an assemblage of Euler–Bernoulli beams connected throughout their length by distributed springs, whose stiffness is governed by the van der Waals force acting between the nanotubes. The spectral element is developed using the recently developed formulation strategy based on the solution of polynomial eigenvalue problem (PEP). A single element can model a MWNT with any number of walls. Studies are carried out to investigate the effect of the number of walls on the spectrum and dispersion relation. Effect of the number of walls on the frequency response function is investigated. Response of MWNT for terahertz level loading is analyzed for broad-band shear pulse.

Keywords: Multi-wall CNT; Wave propagation; Spectral finite element; SVD; polynomial eigenvalue problem

1. Introduction

Starting from their discovery in 1991, carbon nanotubes (CNTs) are continuously subjected to a great deal of theoretical and experimental attention (Tomanek and Enbody, 2000). By virtue of their special symmetric structures, CNTs possess extraordinary mechanical properties, such as extremely high specific strength, specific stiffness, resilience and enormous electrical and thermal conductivities (Tersoff and Ruoff,

* Corresponding author. Tel.: +91 80 22942757 fax: +91 80 3600134.
E-mail address: krishnan@aero.iisc.ernet.in (S. Gopalakrishnan).

0020-7683/$ - see front matter © 2005 Elsevier Ltd. All rights reserved.
doi:10.1016/j.ijsolstr.2005.03.044

1994, Yakobson et al., 1996a, Treacy et al., 1996, Halicioglu, 1998, Harris, 1999, Govindjee and Sackman, 1999, Yoon et al., 2003a). These points, together with other distinctive physical properties, result in many prospective applications, such as strong, light and high toughness fibers for nanocomposites, parts of nanodevices, hydrogen storage (high frequency) micromechanical oscillator, etc.(Iijima, 1991, Dresselhaus and Avouris, 2001, Avouris et al., 1999, Yang et al., 2002, Zheng and Jiang, 2002). However, to exploit these excellent properties for the benefit of mechanical applications, it is necessary to have the fundamental understanding of the nanostructured materials.

Besides an impressive experimental work on CNTs, many researchers have pursued the analysis of carbon nanotubes by theoretical modeling (Harris, 1999, Saito et al., 1998). There are two major approaches in the theoretical modeling of CNTs. One is the atomistic modeling and the major techniques include classical molecular dynamics (MD) (Iijima et al., 1996, Yakobson et al., 1997), tight-binding molecular dynamics (TBMD) (Hernandez et al., 1998) and density functional theory (DFT) (Sanchez-Portal et al., 1999). In principle, any problem associated with molecular or atomic motions can be simulated by these modeling techniques. However, due to their huge computational tasks, practical applications of these atomistic modeling techniques are limited to systems containing a small number of molecules or atoms and are usually connected to studies of relatively short-lived phenomena, from pico-seconds to nanoseconds.

The other approach is the continuum mechanics modeling. Some researchers have resorted to classical continuum mechanics for modeling carbon nanotubes. For examples, Tersoff (1992) conducted simple calculations of the energies of fullerenes based on the deformation of a planar graphite sheet, treated as an elastic continuum, and concluded that the elastic properties of the graphite sheet can be used to predict the elastic strain energy of fullerenes and nanotubes. Yakobson et al. (1996a,b) noticed the unique features of fullerenes and developed a continuum shell model, where the analytical expressions for the energy of a shell in terms of local stresses and deformations were provided. The parameters entering these expressions were obtained from atomistic simulations. The various deformation modes and critical strains were calculated analytically and found to be in good agreement with the results of the microscopic studies. Ru (2000c,d) followed this continuum shell model to investigate buckling of CNTs subjected to axial compression. This kind of continuum shell models can be used to analyze the static or dynamic mechanical properties of nanotubes. However, these models neglect the detailed characteristics of nanotube chirality, and are unable to account for forces acting on the individual atoms. Govindjee and Sackman (1999) used Bernoulli Euler beam bending theory to investigate the applicability of continuum theory to an atomic system such as a nanotube. They emphasize that the tube should be broken down in a number of parallel cross-sections, rather than described as a rigid sheet or rod as had often been assumed. Similarly, Ru (2000a) also observed that the continuum shell postulates break down once atomistic dimensions are reached. Thus, attempts to reconcile continuum theory with atomistic simulations (Yakobson et al., 1996a) had to use parameters, such as the effective thickness of the shell, whose physical origin was itself doubtful. A clear breakdown of the continuum theory occurs when the tube undergoes plastic deformation, since the continuum model is insensitive to the chirality of the wrapping index. However, the continuum approximation can be very valuable and may be the only feasible approach for large and complex systems, but its applicability deserves further scrutiny.

Continuum elastic beam models have been effectively used to study vibrations (Treacy et al., 1996, Poncharal et al., 1999, Yoon et al., 2002, Yoon et al., 2003b) and sound wave propagation (Popov and Doren, 2006, Yoon et al., 2003a) in CNTs. In most previous works, multi-wall nanotubes (MWNTs) have been modeled as single-Euler-elastic-beam (Treacy et al., 1996, Poncharal et al., 1999, Popov and Doren, 2006), which ignored non-coaxial intertube radial displacements and assumed that the nested tubes of an MWNT deform coaxially and thus can be described by a single deflection curve.

Recently, several studies have come up that deal with the role of non-coaxial interlayer radial displacements in transverse vibration (Yoon et al., 2002, Yoon et al., 2003b) and wave propagation (Yoon et al., 2003a) in MWNTs using the multiple-Euler-beam model (Ru, 2000b). The results (Yoon et al.,

2002, Yoon et al., 2003b, Yoon et al., 2003a) showed that non-coaxial intertube vibration and transverse waves of MWNTs will be excited at ultrahigh frequencies (above 1 THz), which would have substantial effects on both the natural frequencies and the wave speed of MWNTs. In view of growing interest in terahertz vibrations and waves of nanoscale materials and devices (Dragoman and Dragoman, 2001, Sirtori, 2002, Jeon and Kim, 2002, Antonelli and Maris, 2002, Knap et al., 2002, Su et al., 2002, Feurer et al., 2003), it is relevant to systematically study terahertz wave propagation in individual MWNTs.

Spectral finite element method (SFEM) (Doyle, 1997) is arguably the most suitable technique for studying wave propagation in structural waveguides due to high frequency content loading. As shown in the study of wave propagation of MWNT (Yoon et al., 2002), the cut-off frequencies appear at tera-Hertz level. Thus, to have contribution from the higher modes, it is necessary to apply loading with frequency content in that level. For this kind of loading, the wave propagation analysis by conventional finite element method (FEM) will prove to be computationally prohibitive, since the element size should be of the order of wavelength (which is nanometer in the present case). However, this problem is totally absent in the SFEM. In this case, the governing equation is transformed first in frequency domain using discrete Fourier transform (DFT). In doing so the governing partial differential equation (PDE) is reduced to a set of ordinary differential equations (ODE) with constant coefficients, where the time coordinate gives way to the frequency, which is introduced as a parameter. The resulting ODEs can be solved exactly. The elements are formulated using the exact solution of the governing ODEs as interpolating polynomials. The use of the exact solution results in exact mass distribution and in turn, the exact dynamic stiffness matrix. Hence, in absence of any discontinuity or irregularity in geometry, one element is sufficient to handle a structure of any length. This feature substantially reduces the size of the global dynamic stiffness matrix to be inverted and the size is many order smaller than the sizes involved in the conventional FEM. The steps to be followed in SEM are as follows: first, the exact dynamic stiffness is used to determine the system transfer function (frequency response function, FRF). The FRF is then convolved with the Fourier coefficients of the load. Next, Inverse Fast Fourier transform (IFFT) is used to get the time history of the response. Most of the developments in isotropic one-dimensional structural waveguide are discussed in the primary book by Doyle (1997).

In the SFEM, in order to obtain the exact solution in the frequency domain, it is necessary to compute two quantities, called the wavenumbers (wave vectors) and the wave amplitudes. In the initial development stage of the SFEM, these quantities are solved manually, and finding solutions for higher order waveguides, e.g., higher order beams, plates and shells, it was impossible to construct the solutions. However, recently two new methods have been proposed to remove this difficulty. The first method is based on the method of the companion matrix (to find the wavenumbers) and the Singular Value Decomposition (SVD) technique (to find the wave amplitudes), which is successfully implemented for graded beams with Poisson's contraction (Chakraborty and Gopalakrishnan, 2004). The second method is based on posing the problem as polynomial eigenvalue problem (PEP) (Lancaster, 1969), which is utilized in plate element formulation (Chakraborty and Gopalakrishnan, in press).

In this work, the Euler–Bernoulli beam model is considered for modeling MWNT. Group speeds are determined as a function of the number of walls making the MWNT, which facilitates to get deep insight in the wave propagation response of MWNTs. The present element formulation exploits the PEP method extensively, which is most suitable in the present case of element formulation as number of walls has been taken as a parameter in element formulation.

The organization of the paper is as follows. In Section 2, the details of the element formulation is presented. General methods are presented for element formulation as well as and to obtain the expressions of cut-off frequencies, spectrum relation and dispersion relation. Section 3 discusses the effect of number of walls on the spectrum and dispersion relation, on the FRF and the wave propagation response due to applied tip shear loading.

2. Mathematical formulation

2.1. Multi-wall beam model

The multiple-elastic beam model for N-walled CNT, based on the Euler–Bernoulli beam theory, is governed by the following set of N-coupled equations

$$c_1[w_2 - w_1] = EI_1 \frac{\partial^4 w_1}{\partial x^4} + \rho A_1 \frac{\partial^2 w_1}{\partial t^2},$$

$$c_p[w_{p+1} - w_p] - c_{p-1}[w_p - w_{p-1}] = EI_p \frac{\partial^4 w_p}{\partial x^4} + \rho A_p \frac{\partial^2 w_p}{\partial t^2}, \quad p = 2 \ldots N-1,$$

$$-c_{N-1}[w_N - w_{N-1}] = EI_N \frac{\partial^4 w_N}{\partial x^4} + \rho A_N \frac{\partial^2 w_N}{\partial t^2},$$

where x is the axial coordinate of the beam, t time, $w_p(x,t)$ $(p = 1, \ldots, N)$ is the deflection of the pth CNT, I_p and A_p are the moment of inertia and the area of the cross-section of the pth tube. Young's modulus $E = 1$ TPa (with the effective thickness 0.35 nm) and the mass density $\rho = 1.3$ g/cm^3. The interaction coefficients c_p $(p = 1, \ldots, N-1)$, arising due to van der Waals interaction between any two adjacent layer, can be estimated approximately as (Yoon et al., 2003a),

$$c_p = \frac{400 R_p \text{ erg/cm}^2}{0.16 d^2}, \quad d = 0.142 \text{ nm}, \ \ p = 1, \ldots, N-1,$$

where R_p is the inner radius of the pth wall. The coefficients c_p have been estimated as the second derivative of the energy-interlayer spacing relations of two flat monolayers. Hence it does not take the curvature effect of CNTs into account.

2.2. Computation of wavenumbers and speeds

The spectral formulation begins by assuming the displacement field as a synthesis of plane waves of the form

$$w_p(x,t) = \sum_{n=1}^{N_q} \tilde{w} \mathrm{e}^{-\mathrm{j}kx} \mathrm{e}^{-\mathrm{j}\omega_n t}, \tag{1}$$

where k is the wavenumber, ω_n is the circular frequency at nth sampling point and $\mathrm{j}^2 = -1$. The N_q is the frequency index corresponding to the Nyquist frequency in fast Fourier transform (FFT) and inverse-FFT (IFFT) used for conversion between time and frequency domain. When Eq. (1) is substituted in the governing equations (GE) the resulting discretized form of the GE becomes

$$c_1(\tilde{w}_2 - \tilde{w}_1) - (EI_1 k^4 - \rho A_1 \omega^2)\tilde{w}_1 = 0,$$

$$c_p(\tilde{w}_{p+1} - \tilde{w}_p) - c_{p-1}(\tilde{w}_p - \tilde{w}_{p-1}) - (EI_p k^4 - \rho A_p \omega^2)\tilde{w}_p = 0, \quad p = 2 \ldots N-1,$$

$$-c_{N-1}(\tilde{w}_N - \tilde{w}_{N-1}) - (EI_N k^4 - \rho A_N \omega^2)\tilde{w}_N = 0,$$

which can be written in the form of a polynomial eigenvalue problem (PEP) as

$$(k^4 \mathbf{A}_4 + \mathbf{A}_0)\mathbf{v} = \mathbf{W}\mathbf{v} = 0, \quad \mathbf{v} = \{w_1, \ldots, w_N\} \tag{2}$$

where $\mathbf{A}_4$ and $\mathbf{A}_0$ are $N \times N$ matrices given by

$$\mathbf{A}_4 = \mathrm{diag}(EI_p,\ p = 1, \ldots, N), \quad \mathbf{A}_0 = \mathbf{C} - \omega^2 \mathbf{M}.$$

Further the matrices $\mathbf{M}$ and $\mathbf{C}$ are defined as

$$\mathbf{M} = \mathrm{diag}(\rho A_p,\ p = 1, \ldots, N), \quad \mathbf{C} = \mathscr{A}_{n=1}^{N}(\mathbf{c}_n),$$

where $\mathscr{A}$ is an assembly operator (like the stiffness matrix assembler of a rod element) and the matrix $\mathbf{c}_n$ is defined as

$$\mathbf{c}_n = \begin{bmatrix} c_n & -c_n \\ -c_n & c_n \end{bmatrix}.$$

On solving Eq. (2), the eigenvalues k and the eigenvectors $\mathbf{v}$ can be obtained, which will be used in subsequent element formulation. Since, in the PEP, the coefficient matrices of k, k^2 and k^3 are zero, we can minimize the cost of computation by substituting λ for k^4 in Eq. (2) and the solving the PEP as a generalized eigenvalue problem

$$\mathbf{A}_0 \mathbf{v} = \lambda(-\mathbf{A}_4)\mathbf{v}$$

and the desired wavenumbers can be expressed as ± 1 and $\pm \mathrm{j}$ times $\lambda^{1/4}$. However, the eigenvectors obtained in this method will be of no consequence and the real eigenvectors need to be computed in a different way.

For a N walled nanotube there are $4N$ wavenumbers and corresponding N phase speeds (c_p) and group speeds (c_g). The phase speeds are defined as ω/k and the group speeds are defined as $\mathrm{d}\omega/\mathrm{d}Re(k)$, where Re denotes real part of an imaginary number. Although the phase speeds can be computed directly from the wavenumbers, it is difficult to compute the group speeds. In this work, they are computed using the characteristic equation (also called the dispersion relation whose roots are the wavenumbers, k), which is given by

$$\phi(k) = \det(k^4 \mathbf{A}_4 + \mathbf{A}_0) = 0.$$

These equations are polynomials in k, whose general form is

$$\phi(k) = \sum_{p=0}^{N} a_p k^{4p},$$

where the coefficients a_p are dependent on material properties and other than a_0, all are functions of ω. Differentiating $\phi(k)$ with respect to k, and using the definition of the expression for c_g is

$$c_g = -\frac{\sum_{p=1}^{N}(4p a_p k^{4p-1})}{\sum_{p=1}^{N}(a'_p k^{4p})},$$

where a'_p indicates derivative of a_p with respect to ω. While computing the group speed using this expression it is to be remembered that for $Re(k) \leqslant 0$, the group speed will be zero.

2.3. Computation of cut-off frequencies

One characteristic of this multi-wall beam based model is that there are $N - 1$ frequencies, where the wavenumber becomes zero, thus rendering the group speed equals to zero and phase speed escapes to infinity. These frequencies are called the cut-off frequencies, whose expression can be obtained by substituting $k = 0$ in the dispersion relation and solving for k. However, for large N, the problem of root finding of a polynomial becomes a cumbersome task (even if we use the companion matrix based technique, we have to

form the related matrices). The problem becomes simple if $k = 0$ is substituted in the Eq. (2) and the problem of finding ω is identified as another PEP

$$(\mathbf{C} - \omega^2\mathbf{M})\mathbf{x} = \mathbf{0},$$

where $\mathbf{x}$ is a hypothetical eigenvector of no consequence in our subsequent formulation. For $N = 2$, there is one cut-off frequency given by

$$\omega_c = \left[\frac{c_1(A_1 + A_2)}{\rho A_1 A_2}\right]^{1/2}, \tag{3}$$

which for equal cross-sectional properties reduces to $2c_1/(\rho A)$ (as given in Doyle (Doyle, 1997)).

2.4. Computation of wave amplitudes

For the spectral element formulation, it is essential to know the eigenvectors $\mathbf{v}$ of the PEP given in Eq. (2), which is also known as the wave vectors. This PEP can be solved directly by the method of linearization for obtaining $\mathbf{v}$ or the method of singular value decomposition (SVD) can be adopted. In the first method, the PEP is converted to a generalized eigenvalue problem in terms of the matrices $\mathbf{A}_4$ and $\mathbf{A}_0$. The matrices are constructed in the following way. If the PEP is posed as

$$\Psi(\lambda)x = (\lambda^\ell \mathbf{A}_\ell + \lambda^{\ell-1}\mathbf{A}_{\ell-1} + \cdots + \lambda\mathbf{A}_1 + \mathbf{A}_0)x = 0, \quad \mathbf{A}_\ell \in \mathbb{C}^{m\times m}$$

then the problem is linearized to

$$\mathbf{A}z = \lambda\mathbf{B}z, \quad \mathbf{A}, \mathbf{B} \in \mathbb{C}^{\ell m\times \ell m} \tag{4}$$

where

$$\mathbf{A} = \begin{bmatrix} 0 & \mathbf{I} & 0 & \cdots & 0 \\ 0 & 0 & \mathbf{I} & \cdots & 0 \\ \vdots & \vdots & \ddots & \ddots & \vdots \\ \vdots & \vdots & \ddots & \ddots & \mathbf{I} \\ -\mathbf{A}_0 & -\mathbf{A}_1 & \mathbf{A}_2 & \cdots & -\mathbf{A}_{\ell-1} \end{bmatrix}, \mathbf{B} = \begin{bmatrix} \mathbf{I} & & & & \\ & \mathbf{I} & & & \\ & & \ddots & & \\ & & & \mathbf{I} & \\ & & & & -\mathbf{A}_\ell \end{bmatrix}$$

and the relation between x and z is given by $z = (x^{\mathrm{T}}, \lambda x^{\mathrm{T}}, \ldots, \lambda^{\ell-1}x^{\mathrm{T}})^{\mathrm{T}}$. $\mathbf{B}^{-1}\mathbf{A}$ is a block companion matrix of the PEP. The generalized eigenvalue problem of Eq. (4) can be solved by the QZ algorithm, iterative method, Jacobi–Davidson method or the rational Krylov method. Each one of these has its own advantages and deficiencies, however, the QZ algorithm is the most powerful method for small to moderate sized problems and hence for the present problem, as the order of the matrices $\mathbf{A}$ and $\mathbf{B}$ is not large ($\ell = 4$, $m = N$). The computation can be performed by the economic and efficient subroutines available in LAPACK (xGGEV and xGGES group).

In the second method, it is noted that $\mathbf{v}$ are the elements of the null space of the matrix $\mathbf{W}$ (which has nontrivial elements as the matrix is singular). In the SVD, $\mathbf{W}$ is factorized as $\mathbf{W} = \mathbf{U}\,\mathbf{S}\mathbf{V}^H$, where $\mathbf{S}$ is a diagonal matrix containing the singular values. Since, $\mathbf{W}$ is singular, there will be zero diagonal elements in $\mathbf{S}$ and the columns of $\mathbf{V}$ correspond to the zero singular values are the elements of the null space of $\mathbf{W}$ (actually they form a basis for the null space). The SVD can be performed by the LAPACK subroutines (xGESVD group).

The wave vectors (eigenvectors) form the matrix of wave amplitudes which is a matrix of size $N \times 4N$. For $N = 2$ and equal cross-sectional properties, the wave amplitude matrix $\mathbf{R}$ is given in closed form as

$$\mathbf{R} = \begin{bmatrix} 1 & 1 & 1 & 1 & 1 & 1 & 1 & 1 \\ 1 & 1 & -1 & -1 & 1 & 1 & -1 & -1 \end{bmatrix},$$

where the order of wavenumbers are as k_1, jk_1, k_2, jk_2 (which are the forward moving waves) and their negative counterparts (which are the backward moving waves). Once the wave matrix is prepared, the total solution is obtained by taking a linear combination of all the $4N$ solutions as

$$\tilde{w}_m(x,\omega_n) = \sum_{n=1}^{4N} R_{mn} \mathrm{e}^{-\mathrm{j}k_n x} a_n, \quad m = 1,\ldots,N, \tag{5}$$

where a_n are the constants to be determined. There are two elements that can be prepared using this solution.

2.5. Finite length spectral element

For this element, the solution given in Eq. (5) is taken as a whole, i.e., both the forward and backward moving wavenumbers are considered. The unknowns, a_n are to be replaced by the nodal variables, which are the transverse displacement and rotation for each wall. Thus, each node has $2N$ degrees of freedom (dofs) and the two noded element has $4N$ dofs (see Fig. 1c). Since, it is the Euler–Bernoulli theory, the rotation is given in terms of derivative of the transverse displacement w_m. The nodal variables of the first and second node are arranged as $\{w_1, \theta_1, \ldots, w_N, \theta_N\}$ and they are collectively referred as $\mathbf{u}_1$ and $\mathbf{u}_2$. Using Eq. (5), the relation between nodal displacement $\tilde{u}$ and the constants $\mathbf{a} = a_m$ are expressed as

$$\tilde{\mathbf{u}} = \begin{Bmatrix} \mathbf{u}_1 \\ \mathbf{u}_2 \end{Bmatrix} = \mathbf{T}_1 \mathbf{a}, \tag{6}$$

where $\mathbf{T}_1$ is a $4N \times 4N$ matrix. As an example, for $N = 2$, the $\mathbf{T}_1$ is given as

$$\mathbf{T}_1 = \begin{bmatrix} R_{11} & R_{12} & \cdots & R_{18} \\ -\mathrm{j}k_1 R_{11} & -\mathrm{j}k_2 R_{12} & \cdots & -\mathrm{j}k_8 R_{18} \\ R_{21} & R_{22} & \cdots & R_{28} \\ -\mathrm{j}k_1 R_{21} & -\mathrm{j}k_2 R_{22} & \cdots & -\mathrm{j}k_8 R_{28} \\ R_{11}e_1 & R_{12}e_2 & \cdots & R_{18}e_8 \\ -\mathrm{j}k_1 R_{11}e_1 & -\mathrm{j}k_2 R_{12}e_2 & \cdots & -\mathrm{j}k_8 R_{18}e_8 \\ R_{21}e_1 & R_{22}e_2 & \cdots & R_{28}e_8 \\ -\mathrm{j}k_1 R_{21}e_1 & -\mathrm{j}k_2 R_{22}e_2 & \cdots & -\mathrm{j}k_8 R_{28}e_8 \end{bmatrix},$$

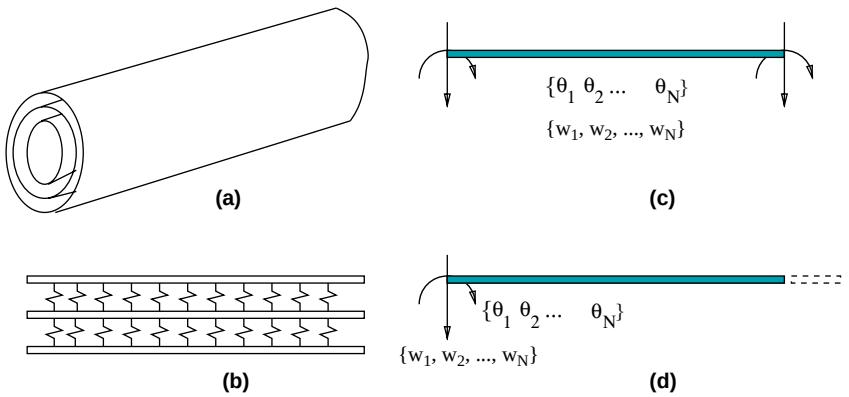

Fig. 1. Spectral element model for MWNT: (a) 3-wall CNT; (b) its beam model; (c) finite length spectral element and (d) semi-infinite spectral element.

where $e_i = \exp(-\mathrm{j}k_i L)$. Next, the relation between the nodal displacements and forces needs to be established. The nodal forces are the shear force (V) and bending moment (M) acting at transverse and rotational dof, respectively. At each node there are N shear forces and N bending moments, which are related to the displacement field by the relation

$$M_p = EI_p \frac{\partial^2 w_p}{\partial x^2}, \quad V_p = -EI_p \frac{\partial^3 w_p}{\partial x^3}, \ p = 1, \ldots, N.$$

Using the above relationship, the nodal forces $\mathbf{f}_1$ and $\mathbf{f}_2$ are evaluated at the nodes at $x = 0$ and $x = L$, respectively, as

$$\mathbf{f}_1 = \{-V_1(0), -M_1(0), \ldots, -V_N(0), -M_N(0)\},$$

$$\mathbf{f}_2 = \{V_1(L), M_1(L), \ldots, V_N(L), M_N(L)\},$$

which are related to the constants $\mathbf{a}$ by the relation

$$\tilde{\mathbf{f}} = \begin{Bmatrix} \mathbf{f}_1 \\ \mathbf{f}_2 \end{Bmatrix} = \mathbf{T}_2 \mathbf{a}. \tag{7}$$

Combining Eqs. 6 and 7, the relation between the nodal forces and nodal displacements is

$$\tilde{\mathbf{f}} = \mathbf{T}_2 \mathbf{T}_1^{-1} \tilde{\mathbf{u}} = \mathbf{K} \tilde{\mathbf{u}}, \tag{8}$$

where $\mathbf{K}$ is the dynamic stiffness matrix of size $4N \times 4N$. This matrix exactly relates the nodal forces with nodal displacements at frequency ω_n and thus one element should be sufficient to model a uniform tube of any length. In the finite precision computing environment, however, there will be restriction on the length of the element due to the evaluation of e_i.

2.6. Semi-infinite spectral element

While forming the total solution, if only the forward propagating components, i.e., all the positive wavenumbers, are selected, the waveguide will resemble to an infinite structure, which carries no reflection from the other boundary (see Fig. 1d). This element is also called throw-off element as it acts as a conduit for throwing away energy from the structure. The element is useful in modeling large structure and to introduce artificial damping. The displacement field for this element is

$$\tilde{w}_m(x, \omega_n) = \sum_{n=1}^{2N} R_{mn} \mathrm{e}^{-\mathrm{j}k_n x} a_n, \quad m = 1, \ldots, N, \tag{9}$$

which can be used readily to establish the relation between the nodal displacements and forces as

$$\tilde{\mathbf{u}} = \mathbf{u}_1 = \mathbf{T}_1 \mathbf{a}, \quad \tilde{\mathbf{f}} = \mathbf{f}_1 = \mathbf{T}_2 \mathbf{a}, \quad \mathbf{f}_1 = \mathbf{T}_2 \mathbf{T}_1^{-1} \mathbf{u}_1,$$

where all the matrices are now of size $2N \times 2N$.

3. Numerical examples

In this section, the efficiency of the developed spectral element is demonstrated. A broad-band pulse loading is applied to study the wave propagation in MWNT. However, before going into the details of the wave propagation simulation, the spectrum and dispersion relation of MWNT is studied for different N and the wave characteristics are discussed in detail.

For all the subsequent numerical examples, MWNT are taken with Young's modulus $E = 1$ TPa, shear modulus $G = 0.4$ TPa and density $\rho = 1300$ kg/m^3. The innermost radius of the tube is taken as 5 nm and each tube is 0.35 nm thick. The van der Waals force interaction coefficient for the first wall becomes 0.62 TPa. This geometric and material properties result in waveforms and wave characteristics, which are given in the following sections.

3.1. Spectrum and dispersion relation

The wavenumber, phase speed and group speed variation for $N = 3$ are plotted in Figs. 2–4, respectively. As previously mentioned, there are two cut-off frequencies, one at 1.014 and another at 1.757 THz. At these frequencies, the wavenumber becomes zero and corresponding phase speed becomes infinite and group speed zero. However, before the cut-off frequencies, the wavenumbers (k_2 and k_3) have real as well as imaginary part, which indicates that there are propagating component of these modes. Due to the presence of the imaginary part, these waves will, however, attenuate while propagating. Thus, these waves are the so called inhomogeneous waves. Thus, there are nonzero phase and group speeds before the cut-off frequencies.

For $N = 10$, the spectrum relation and phase speed variation are given in Figs. 5 and 6, respectively. The characteristic remains same as before, where now appear nine cut-off frequencies. The minimum of them is at 0.2886 THz and the maximum is at 1.891 THz. Thus, it becomes apparent, even for this many number of tubes, there is no great variation in the maximum cut-off frequency. It suggests that there may exist an upper bound to the range of cut-off frequencies and similarly a lower bound. To study this aspect, the number of walls N is varied from 2 to 100 and for these values the maximum and the minimum cut-off frequencies are plotted in Fig. 7. The figure suggests that, indeed there are an upper and lower bound of the cut-off frequencies, which, for this particular material and geometric parameters are at 1.891 THz and 0.0169 THz.

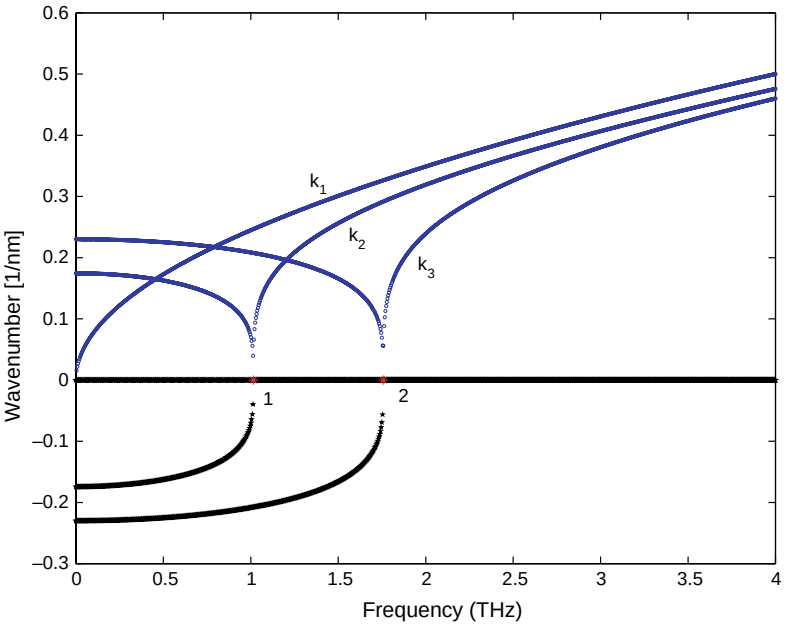

Fig. 2. Wavenumber variation for $N = 3$.

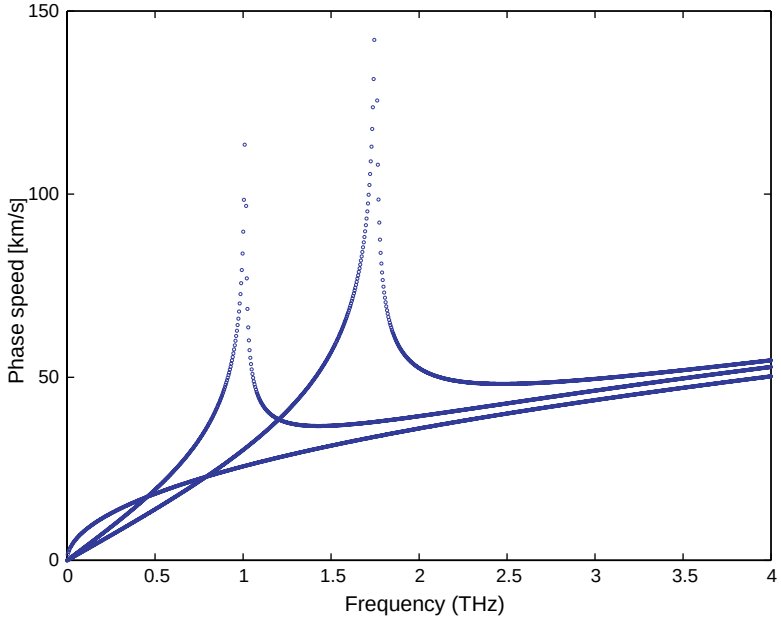

Fig. 3. Phase speed variation for $N = 3$.

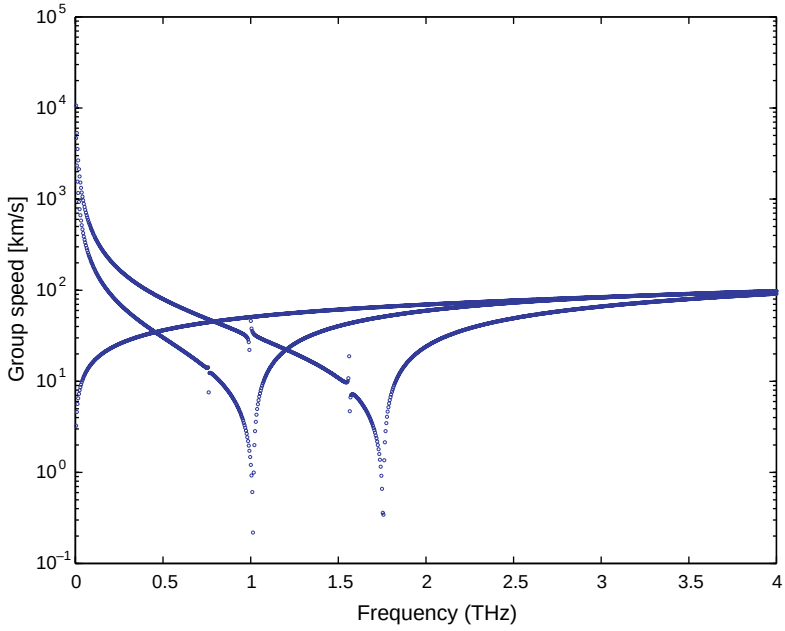

Fig. 4. Group speed variation for $N = 3$.

Since there is no appreciable difference in cut-off frequencies with wall numbers, an MWNT can be approximated by a double-wall nanotube (DWNT), where the effective inner radius of the DWNT can

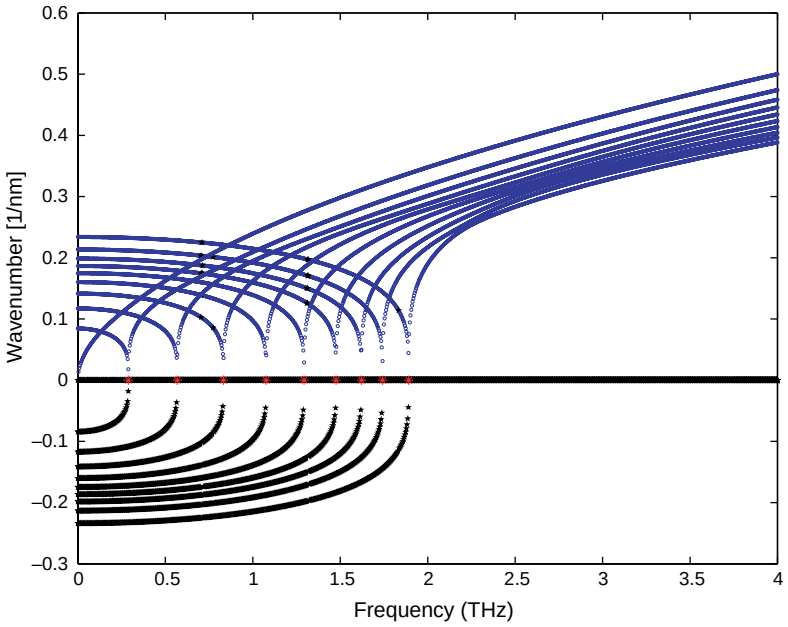

Fig. 5. Wavenumber variation for $N = 10$.

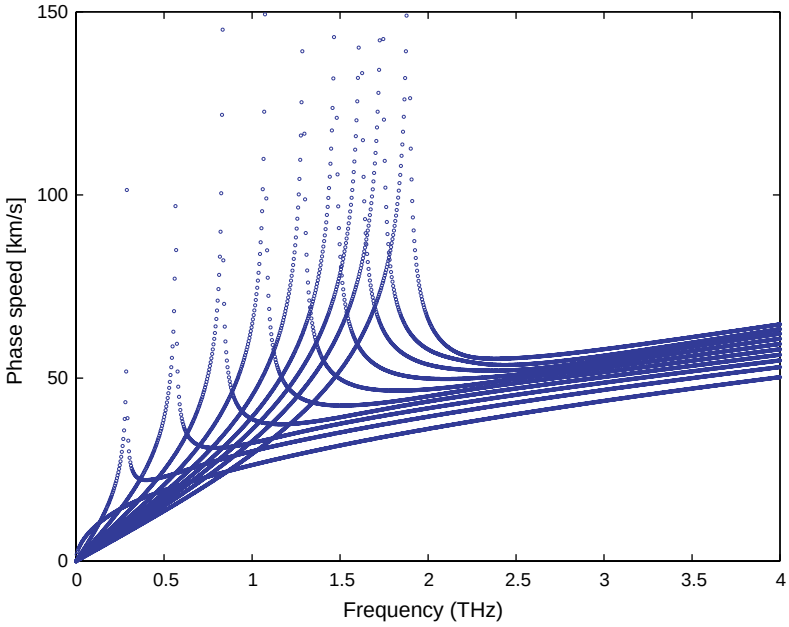

Fig. 6. Phase speed variation for $N = 10$.

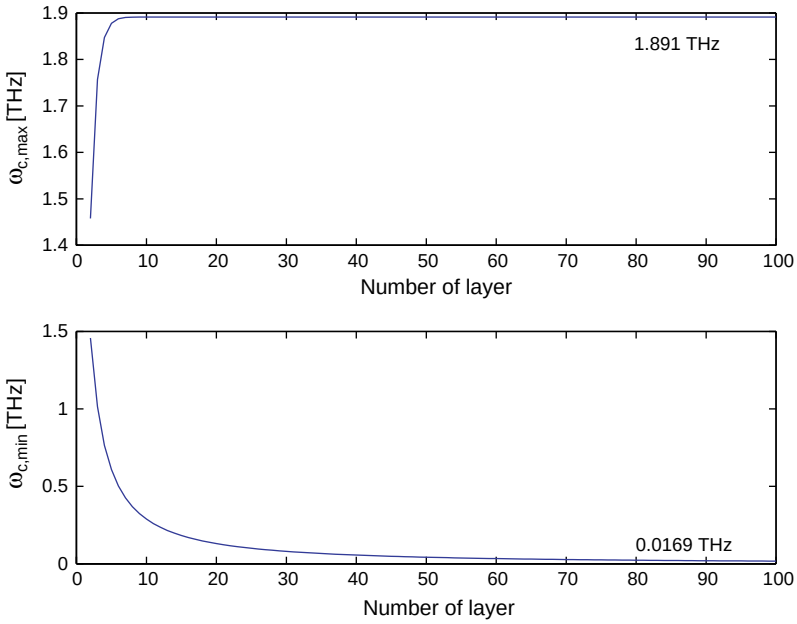

Fig. 7. Variation of the maximum and minimum cut-off frequencies with N.

be obtained from the magnitudes of the maximum and minimum cut-off frequencies. For example, in the present case, for a identical DWNT, the inner radius will be 1.737 nm, which is obtained using the maximum cut-off frequency and Eq. (3).

3.2. Variation of frequency response function (FRF)

Before considering any particular loading it is expedient to study the FRF for some particular loading and dof. To this end a cantilever MWNT of length 250 nm is considered. The tube is impacted at the free end in the transverse direction equally in all the transverse dof. The FRF of the transverse velocity (corresponding to w_1) is plotted in Fig. 8 for N varying from 1 to 3. The FRF clearly shows how the natural frequencies shift with increasing number of tubes, which is evident since the stiffness of the structure increases.

Similarly, for an applied moment at the free end, the FRF of the rotational velocity (corresponding to θ_1) shows similar characteristics, which is shown in Fig. 9.

3.3. Effect of broad-band pulse loading

Once the characteristics of the waves are known, real time data can be obtained by the application of small duration loading of suitable frequency content. A broad-band pulse is considered with a frequency content of around 2.1 THz (see Fig. 10), which is above the highest cut-off frequency for any N. The time domain data of the loading is shown in the inset. As the figure suggests, the load starts at 2 ps and completes by 3 ps within which it attains a maximum magnitude of unity. This load is applied at the free end of a cantilever MWNT and the responses are measured at the tip. The load is equally distributed at all the tubes so that the total load is always 1 nN.

The transverse velocity history at the tip of the beam is shown in Fig. 11 for different wall numbers. The initial peak is the instantaneous effect of the loading, whereas, the oscillations at the later part is the reflec-

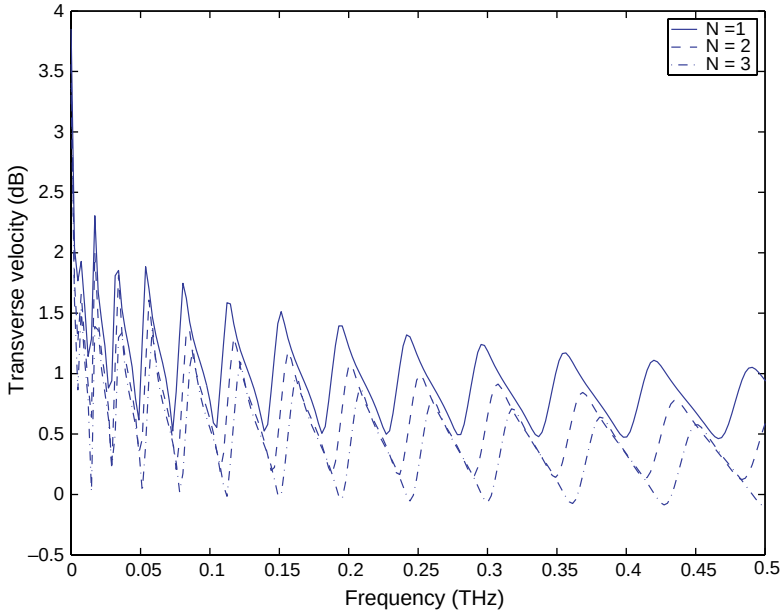

Fig. 8. Frequency response function of cantilever tube.

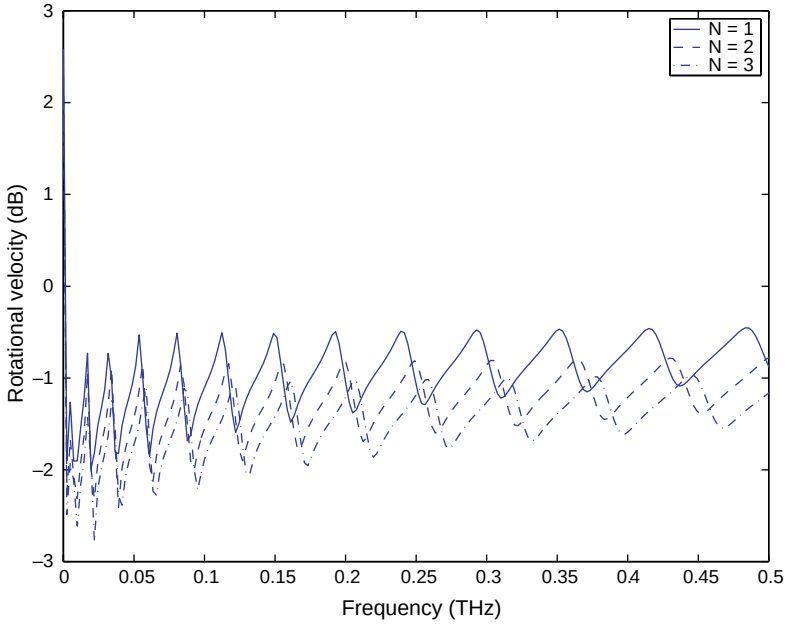

Fig. 9. Frequency response function of cantilever tube.

tion from the fixed end. As the figure suggests, with increasing N, the overall stiffness increases considerably and group speed decreases as evident from the decreasing magnitude and arrival time of the boundary reflections.

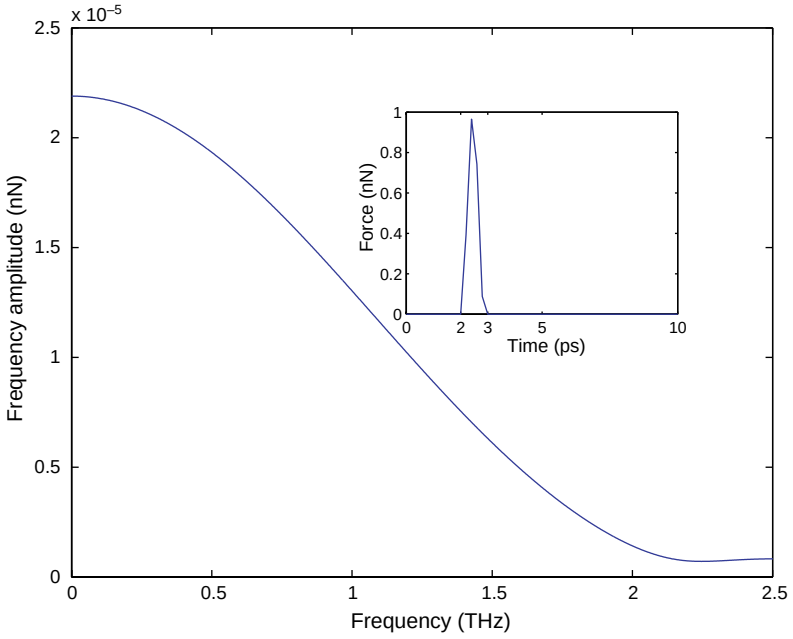

Fig. 10. Broad-band pulse loading.

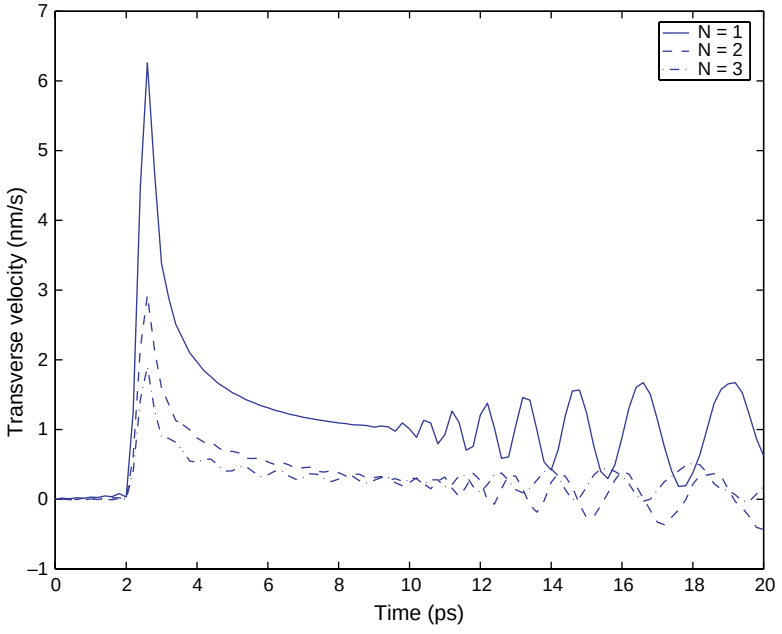

Fig. 11. Transverse velocity due to end shear force.

4. Conclusion

A new spectral element is formulated, which can effectively model MWNTs. The element can have any number of walls and the essential wave propagation characteristics, in terms of cut-off frequencies, group speed variation etc. are inbuilt in the element formulation. The formulation also reveals the effect of the number of walls on the wavenumber, phase speed and group speed variation. It is found that a N wall MWNT will have $N-1$ cut-off frequencies. More importantly, the maximum and minimum values of these frequencies are independent of the number of layers. The study of FRF shows that with increasing wall number, the natural frequencies increase and the effect is more pronounced in the higher modes. Response of MWNT for point shear loading clearly shows the effect of wall number in terms of high stiffness and low group speed.

References

Antonelli, G., Maris, H., 2002. Picosecond ultrasonics study of the vibrational modes of a nanostructure. J. Appl. Phys. 91, 3261–3267.

Avouris, P., Hertel, T., Martel, R., Schmidt, T.H.R.H.S., Walkup, R., 1999. Carbon nanotubes: nanomechanics, manipulation, and electronic devices. Appl. Surf. Sci. 1999, 201–209.

Chakraborty, A., Gopalakrishnan, S., 2004. A higher order spectral element for wave propagation analysis in functionally graded materials. Acta Mech. 172 (1–2), 17–43.

Chakraborty, A., Gopalakrishnan, S., in press. A spectrally formulated plate element for wave propagation analysis in anisotropic material. Comput. Methods Appl. Mech. Eng.

Doyle, J.F., 1997. Wave Propagation in Structures. Springer, Berlin.

Dragoman, D., Dragoman, M., 2001. Micro/nano-optoelectromechanical systems. Prog Quant Electron 25, 229–290.

Dresselhaus, M.S.G.D., Avouris, P., 2001. Carbon nanotubes. Top. Appl. Phys. 80, 287–329.

Feurer, T., Vaughan, J., Nelson, K., 2003. Spatiotemporal coherent control of lattice vibrational waves. Science 299, 374.

Govindjee, S., Sackman, J., 1999. On the use of continuum mechanics to estimate the properties of nanotubes. Solid State Commun. 110 (4), 227–230.

Halicioglu, T., 1998. Stress calculation for carbon nanotubes. Thin Solid Films 312 (1–2), 11–14.

Harris, P., 1999. Carbon Nanotubes and Related Structures. Cambridge University Press, Cambridge, MA.

Hernandez, E., Goze, C., Bernier, P., Rubio, A., 1998. Elastic properties of C and $B_xC_yN_z$ composite nanotubes. Phys. Rev. Lett. 80, 4502–4505.

Iijima, S., 1991. Helical microtubes of graphitic carbon. Nature 354, 56–58.

Iijima, S., Brabec, C., Maiti, A., Bernholc, J., 1996. Structural exibility of carbon nanotubes. J. Chem. Phys. 104, 2089–2092.

Jeon, T., Kim, K., 2002. Terahertz conductivity of anisotropic single walled carbon nanotube films. Appl. Phys. Lett. 80, 3403–3405.

Knap, W., Kachorovskii, V., Deng, Y., Rumyantsev, S., Lu, J., Gaska, R., Shur, M., 2002. Nonresonant detection of terahertz radiation in field effect transistors. J. Appl. Phys. 91, 9346–9353.

Lancaster, P., 1969. Theory of Matrices. Academic Press, New York.

Poncharal, P., Wang, Z., Ugarte, D., de Heer, W., 1999. Electrostatic deflections and electromechanical resonances of carbon nanotubes. Science 283, 1513–1516.

Popov, V., Doren, V., 2006. Elastic properties of single-walled carbon nanotubes. Phys. Rev. B 61, 3078–3084.

Ru, C., 2000a. Effective bending stiffness of carbon nanotube. Phys. Rev. B 62 (15), 9973–9976.

Ru, C.Q., 2000b. Column buckling of multiwalled carbon nanotubes with interlayer radial displacements. Phys. Rev. B 62, 16962–16967.

Ru, C.Q., 2000c. Effective bending stiffness of carbon nanotubes. Phys. Rev. B 62, 9973–9976.

Ru, C.Q., 2000d. Elastic buckling of single-walled carbon nanotube ropes under high pressure. Phys. Rev. B 62, 10405–10408.

Saito, S., Dresselhaus, D., Dresselhaus, M., 1998. Physical Properties of Carbon Nanotubes. Imperial College Press, London.

Sanchez-Portal, D., Artacho, E., Soler, J., Rubio, A., Ordejon, P., 1999. Ab initio structural, elastic and vibrational properties of carbon nanotubes. Phys. Rev. B 59, 12678–12688.

Sirtori, C., 2002. Bridge for the terahertz gap. Nature 417, 132–133.

Su, M., Carter, S., Sherwin, M., Huntington, A., Coldren, L., 2002. Voltage-controlled wavelength conversion by terahertz electro-optic modulation in double quantum wells. Appl. Phys. Lett. 81, 1564–1566.

Tersoff, J., 1992. Energies of fullerenes. Phys. Rev. B 46, 15546–15549.

Tersoff, J., Ruoff, R., 1994. Structural properties of a carbon-nanotube crystal. Phys. Rev. Lett. 73 (5), 676–679.

Tomanek, D., Enbody, R., 2000. Science and Applications of Nanotubes. Kluwer/Plenum, New York.
Treacy, M., Ebbesen, T., Gibson, J., 1996. Exceptionally high Young's modulus observed for individual carbon nanotubes. Nature 381, 678.
Yakobson, B., Brabec, C., Bernholc, J., 1996a. Nanomechanics of carbon tubes: instabilities beyond linear range. Phys. Rev. Lett. 76, 2511–2514.
Yakobson, B., Brabec, C., Bernholc, J., 1996b. Structural mechanics of carbon nanotubes: from continuum elasticity to atomistic fracture. J. Comput.-Aid. Mater. Design 3, 173–182.
Yakobson, B., Campbell, M., Brabec, C., Bernholc, J., 1997. High strain rate fracture and C-chain unraveling in carbon nanotubes. Computat. Mater. Sci. 8, 341–348.
Yang, W., Ma, X., Wang, H., Hong, W., 2002. Advances in nanomechanics. Adv. Mech. 32, 161–174.
Yoon, J., Ru, C., Mioduchowski, A., 2002. Non-coaxial resonance of an isolated multiwall carbon nanotube. Phys. Rev B 66, 233402.
Yoon, J., Ru, C., Mioduchowski, A., 2003a. Sound wave propagation in multiwall carbon nanotubes. J. Appl. Phys. 93 (8), 4801–4806.
Yoon, J., Ru, C., Mioduchowski, A., 2003b. Vibration of embedded multiwall carbon nanotubes. Compos. Sci. Technol. 63, 1533–1542.
Zheng, Q., Jiang, Q., 2002. Multiwalled carbon nanotubes as gigahertz oscillator. Phys. Rev. Lett. 88, 045503.